SPECIAL MERRA COLLECTION

SPECIAL U.S. CLIVAR SeaFlux COLLECTION

The Moisture Budget of the Polar Atmosphere in MERRA

RICHARD I. CULLATHER

Earth System Science Interdisciplinary Center, University of Maryland, College Park, College Park, Maryland

MICHAEL G. BOSILOVICH

Global Modeling and Assimilation Office, NASA Goddard Space Flight Center, Greenbelt, Maryland

(Manuscript received 21 September 2010, in final form 9 December 2010)

ABSTRACT

The atmospheric moisture budget from the Modern Era Retrospective-Analysis for Research and Applications (MERRA) is evaluated in polar regions for the period 1979–2005 and compared with previous estimates, accumulation syntheses over polar ice sheets, and in situ Arctic precipitation observations. The system is based on a nonspectral background model and utilizes the incremental analysis update scheme. The annual moisture convergence from MERRA for the north polar cap is comparable to previous estimates using 40-yr European Centre for Medium-Range Weather Forecasts Re-Analysis (ERA-40) and earlier reanalyses but it is more than 50% larger than MERRA precipitation minus evaporation ($P - E$) computed from physics output fields. This imbalance is comparable to earlier reanalyses for the Arctic. For the south polar cap, the imbalance is 20%. The MERRA physics output fields are also found to be overly sensitive to changes in the satellite observing system, particularly over data-sparse regions of the Southern Ocean. Comparisons between MERRA and prognostic fields from two contemporary reanalyses yield a spread of values from 6% of the mean over the Antarctic Ice Sheet to 61% over a domain of the Arctic Ocean. These issues highlight continued problems associated with the representation of cold-climate physical processes in global data assimilation models. The distribution of MERRA surface fluxes over the major polar ice sheets emphasizes larger values along the coastal escarpments, which agrees more closely with recent assessments of ice sheet accumulation using regional models. Differences between these results and earlier assessments illustrate a continued ambiguity in the surface moisture flux distribution over Greenland and Antarctica. The higher spatial and temporal resolution as well as the availability of all budget components, including analysis increments in MERRA, offer prospects for an improved representation of the high-latitude water cycle in reanalyses.

1. Introduction

The Modern Era Retrospective-Analysis for Research and Applications (MERRA) has recently been produced by the National Aeronautics and Space Administration's (NASA) Global Modeling and Assimilation Office (GMAO). The objectives of MERRA are to provide a climate context for the NASA satellite-observing system and to improve the representation of the water cycle in reanalyses. Numerical reanalyses have been useful in making the historical record more homogeneous and accessible for many applications (Trenberth et al. 2008). For the Arctic and the Antarctic, atmospheric analyses are important tools for the systematic evaluation of large-scale atmospheric phenomena. Reanalysis fields have been widely used in weather and climate studies of the polar regions because of their utility in marshalling the sparse available observations of these areas into a gridded, coherent, and (arguably) plausible dynamical representation of the atmospheric state. Innovative research has been conducted using reanalyses that have led to an improved understanding of high-latitude teleconnection patterns (e.g., Thompson and Wallace 1998; Hurrell et al. 2001; Genthon et al. 2003; Monaghan and Bromwich 2008) and the identification of prevailing atmospheric conditions during recent, dramatic reductions in Arctic perennial sea ice cover (Ogi and Wallace 2007). Reanalyses are also used as first-order validation for

Corresponding author address: Richard Cullather, ESSIC, University of Maryland at College Park, c/o NASA/GSFC Code 610.1, 8800 Greenbelt Road, Greenbelt, MD 20771.
E-mail: richard.cullather@nasa.gov

DOI: 10.1175/2010JCLI4090.1

© 2011 American Meteorological Society

climate models and provide necessary boundary forcing conditions for ocean–sea ice, land surface, and limited-area atmospheric models (e.g., Walsh et al. 2002; Rinke et al. 2006). Notwithstanding these wide-ranging and constructive applications, reanalyses contain some degree of uncertainty because of the limitations in the observing systems, inconsistencies between differing observations, and incomplete knowledge of the physical processes that are represented in the background weather forecast model (e.g., Thorne 2008; Grant et al. 2008; Bitz and Fu 2008; Hines et al. 2000). An initial evaluation of a reanalysis record is therefore a useful undertaking.

The purpose of this study is to provide a basic overview of the quality of MERRA in polar regions. To this end we focus on the atmospheric moisture budget, which has recently been the subject of other studies. A companion paper examines the representation of the atmospheric energy budget in MERRA over high latitudes (Cullather and Bosilovich 2011, manuscript submitted to *J. Climate*). The surface moisture balance in polar regions, including the large continental ice sheets and sea ice zones, has significant relevance to a wide variety of physical science disciplines with potential importance for understanding eustatic change. Together with the energy balance, these budgets provide an important starting point for evaluating this reanalysis. Some of the questions to be addressed are as follows:

- What are the spatial and temporal patterns of moisture budget components in MERRA, and how do they compare with previous studies?
- How does the MERRA surface moisture flux compare with in situ observations?
- What is the nature of adjustment terms in the budget?

Section 2 provides an overview of the MERRA dataset and method. An evaluation of the surface moisture flux in polar regions is provided in section 3. A discussion of these comparisons is then given in section 4.

2. MERRA description and method

MERRA was made using the data assimilation system component of the Goddard Earth Observing System (GEOS DAS; Rienecker et al. 2008) and covers the modern satellite era from 1979 to the present. The MERRA time series was produced in three segments as described by Rienecker et al. (2011). The assimilation system utilizes the GEOS model, version 5 (GEOS-5)—a finite-volume atmospheric general circulation model (AGCM) that is used for routine numerical weather prediction. For MERRA, the GEOS DAS was run at a horizontal resolution of ⅔° longitude × ½° latitude and 72 hybrid-sigma coordinate vertical levels to produce an observational analysis at 6-h intervals. Prescribed conditions include climatological aerosol and solar forcing. Sea surface temperature and sea ice are linearly interpolated in time from weekly 1°-resolution Reynolds fields (Reynolds et al. 2002). On nonglaciated land, the atmospheric model is coupled to a catchment-based hydrologic model (Koster et al. 2000) and a sophisticated multilayer snow model (Stieglitz et al. 2001) that is coupled to the catchment hydrology. Land surface albedos are derived from retrievals of the Moderate Resolution Imaging Spectroradiometer (MODIS; Moody et al. 2005). MERRA uses the global 30 arc-second elevation dataset (GTOPO30) produced by the Earth Resources Observation and Science (EROS) Center of the U.S. Geological Survey (Gesch 1994).

For each analysis, the system incorporates the state of the background forecast model, which is taken at the analysis time, at 3 h prior and at 3 h after the time, with all the available observations taken over the encompassing 6-h interval to produce gridded fields of state and dynamical variables. The difference between this reference and the background forecast model state is then calculated to produce an analysis tendency (GMAO 2008). The forecast model is then run again over the 6-h interval, with this tendency added as an additional model forcing term. The output fields of this simulation are preserved at 1-hourly intervals. The resulting MERRA product is then composed of dynamically consistent 1-hourly fields that are incrementally corrected to observation every 6 h. One advantage of this method—referred to as the incremental analysis update (IAU; Bloom et al. 1996)—is that it explicitly quantifies adjustment terms in atmospheric balance equations. Thus, atmospheric budgets—as they are constructed in the GEOS-5 AGCM—and their incremental adjustments are maintained within MERRA to the accuracy limited by round-off and data compression errors. This may be contrasted with alternate systems, where a temporal mismatch arises in balance equations between instantaneous analysis fields and forecast variables that are accumulated over some model integration period. The IAU additionally limits model spindown as the GEOS DAS progresses over the 6-h window and allows for the hourly temporal resolution of output variables.

The atmospheric moisture budget for MERRA may be written as

$$\frac{\partial(W_v + W_l + W_i)}{\partial t} + \nabla \cdot \left[\int_{p_{\mathrm{top}}}^{p_{\mathrm{sfc}}} (q_v + q_l + q_i)\tilde{\mathbf{V}}\,\frac{dp}{g}\right] = E - P + \left.\frac{\partial W_v}{\partial t}\right|_{\mathrm{CHM}} + \left.\frac{\partial(W_v + W_l + W_i)}{\partial t}\right|_{\mathrm{FIL}} + \mathrm{ANA}_{(M)}, \tag{1}$$

where

$$W_{(v,l,i)} = \int_{p_{\mathrm{top}}}^{p_{\mathrm{sfc}}} q_{(v,l,i)} \frac{dp}{g}. \quad (2)$$

Here, W_v is the column-integrated water vapor (precipitable water); W_l is the total cloud liquid condensate in the atmospheric column; W_i is the total cloud ice condensate in the atmospheric column; q_v is the specific humidity; q_l is the cloud liquid water mixing ratio; q_i is the cloud ice mixing ratio; p_{sfc} is the surface pressure; p_{top} is the fixed pressure of the top model level, which is 0.01 hPa; $\tilde{\mathbf{V}}$ is the horizontal wind vector; and g is the gravity constant. The symbol E represents the vertical flux of water vapor at the surface, P is the total (solid plus liquid) precipitation, and $\mathrm{ANA}_{(M)}$ is the tendency resulting from the IAU procedure applied to the moisture budget. The first term on the left-hand side represents a temporal derivative and is given by the summation of three MERRA variables for each water species, denoting contributions from model dynamics, physical parameterizations, and the IAU procedure. The relation between MERRA variables and equation notation is detailed in the appendix. The tendency of precipitable water is negligible for the annual mean but may be significant on monthly time scales depending on the local condition. On the right-hand side, the term denoted by the subscript ''CHM'' represents a parameterized source of water vapor in the middle atmosphere from the model chemistry routine and is small (GMAO 2008). The notation ''FIL'' refers to tendencies associated with the ''filling'' of spurious negative water, which was found to be negligible in all cases.

In atmospheric science, the quantity of precipitation minus evaporation ($P - E$) is sometimes referred to as ''net precipitation.'' Disregarding the chemistry and spurious filling terms, it may be seen from (1) that two different measures of net precipitation are obtainable from reanalyses, which differ by the $\mathrm{ANA}_{(M)}$ term. The first measure's values, obtained from the terms on the left-hand side of (1), are derived from analyses of state and dynamic variables in the atmospheric profile and are referred to as the ''aerological method'' (e.g., Serreze et al. 2006). The expression is derived from the use of rawinsonde measurements but suffices for the use of reanalyses atmospheric profiles of moisture content and transport in determining convergence in the atmospheric column. The second measure is obtained from the first two terms on the right-hand side, which are individual output products of the assimilating model's physical parameterizations. For clarity this method is referred to here as the physics output. Studies using other reanalyses, which rely on prognostic fields as described earlier, have used different terminology. Over grounded ice sheets of Greenland and Antarctica, net precipitation may be compared with observed surface accumulation with the knowledge that additional terms, including meltwater runoff, blowing snow horizontal transport, and the sublimation of postprecipitated blowing snow, may be locally large (e.g., Bintanja 1998; Box et al. 2006).

The approach of this work is to evaluate MERRA against prior studies for large-scale areal averages of the terms in (1) over fixed regions of Greenland and Antarctic conterminous grounded ice sheets, sea ice fields, and a particular focus on the polar caps. Corresponding values are also tabulated for two contemporary reanalyses for comparison: the European Centre for Medium-Range Weather Forecasts (ECMWF) Interim Re-Analyses (ERA-I; Simmons et al. 2007) and the U.S. National Centers for Environmental Prediction (NCEP) Climate Forecast System Reanalysis (CFSR; Saha et al. 2010). The ERA-I was produced at T-255 spectral resolution. Precipitation and evaporation fields are produced from 12-h forecasts initialized by four-dimensional variational data assimilation (4D-Var). These fields were obtained on a regular grid at a resolution of 0.7° × 0.7° and then averaged into monthly fields. The ERA-I currently begins in 1989 and was therefore obtained for the overlapping period 1989–2005. The CFSR utilize a coupled atmosphere–ocean model for the initial guess field with an interactive sea ice model and was produced at T-382 spectral resolution. Model variables are produced from 6-h forecasts. Precipitation and latent heat flux fields were obtained at full resolution from the National Climatic Data Center for the period 1979–2005. Evaporation for the CFSR was computed from 6-h prognostic surface latent heat flux fields using snow cover and sea ice conditions to denote the latent heat of phase transition.

The regions of interest are shown in Fig. 1. Historically, budgets of the polar caps have been defined using the 70° parallels as boundaries that roughly correspond to geographical contrasts between land and ocean and a local maximum in the coverage of the in situ observation network. Boundaries composed of parallels have also served for straightforward comparisons with climate models (e.g., Briegleb and Bromwich 1998). An Arctic Ocean domain is also utilized to roughly correspond with the recent study of Serreze et al. (2006). Finally, a Southern Ocean fixed domain is determined by the farthest north wintertime sea ice edge. In support of these budget comparisons, the evaluation of near-surface state variables against station observations is also instructive. The results presented are for the period 1979–2005. Surface moisture flux and accumulation are given in water-equivalent units.

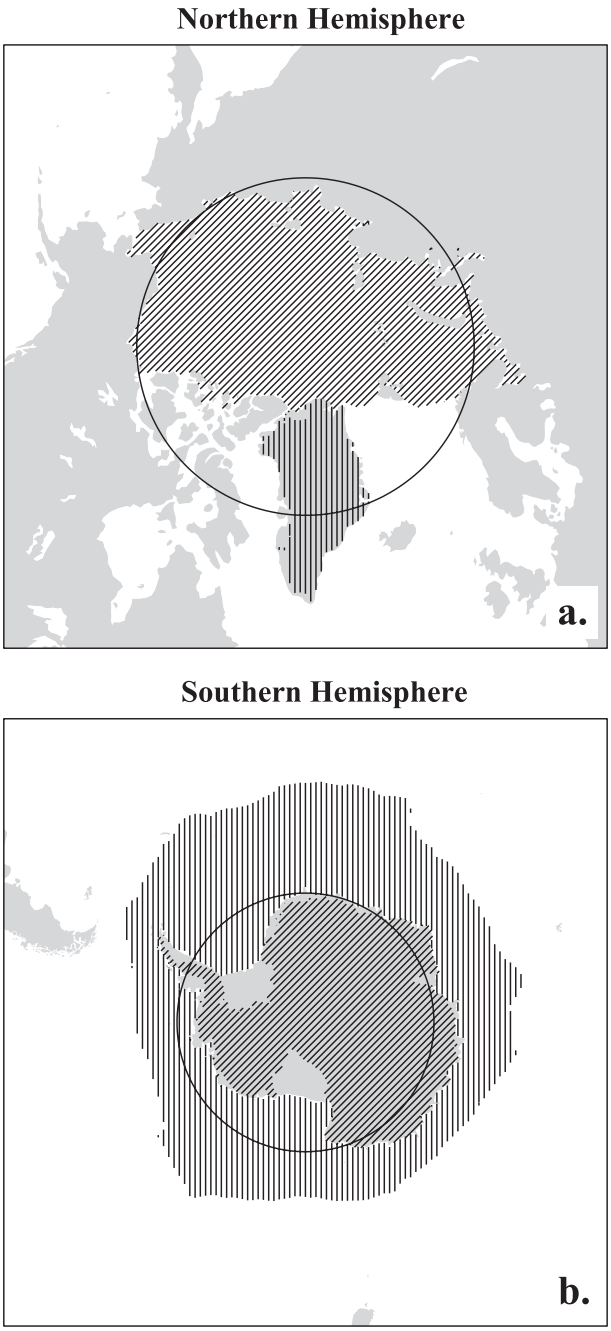

FIG. 1. Regions of study for (a) the Northern Hemisphere and (b) the Southern Hemisphere. Thick line indicates the 70° parallel. Continental areas, which include major ice shelves in Antarctica, are shaded gray.

3. Surface moisture flux

a. Mean distribution and annual cycle

Principal characteristics of the average surface moisture flux over the Northern Hemisphere polar regions are qualitatively represented in the MERRA-averaged moisture convergence field contoured in Fig. 2a and are composed of modest amounts of annual net precipitation over the Arctic Ocean of between 15 and 30 cm yr^{-1}; smaller amounts over land surfaces in northern Canada and Siberia; and local maxima of 100–200 cm yr^{-1} or more over eastern Scandinavia, the Gulf of Alaska, Iceland, and southeastern Greenland. These four areas of maxima are associated with wintertime Atlantic and Pacific storm tracks and lie equatorward of the 70°N parallel. The moisture convergence from MERRA over Greenland reflects a characteristic pattern of the largest values in the southeastern coastal region, contours of large values extending along the western coast, and smaller values in the northern region and over the higher elevations of the ice sheet. Annual-averaged negative values (divergence) are associated with the northernmost reach of the warm-surface Norwegian current as it enters the subpolar gyre near Svalbard. On land, prominent orographic uplift signals are apparent. Values greater than 30 cm yr^{-1} are located to the east of the central Siberian Plateau and decrease to less than 15 cm yr^{-1} in eastern Siberia. Spurious negative values are found over lower-latitude Asian land surfaces. In general, however, the large-scale patterns for the Arctic are qualitatively similar to compiled climatologies, such as the Gorshkov atlas (Gorshkov 1983), and more recent assessments using other reanalyses (e.g., Serreze et al. 2006; Bromwich et al. 2002). For example, average fields of the 40-yr ECMWF Re-Analysis (ERA-40; Uppala et al. 2005) similarly indicate the central Siberian Plateau maxima and annual-averaged moisture divergence near Svalbard (Bromwich et al. 2002).

Figure 3a shows the annual cycle of the moisture balance components for the north polar cap domain. Similar to results for earlier reanalyses shown in Bromwich et al. (2000), the annual cycle of atmospheric moisture convergence for the north polar cap in MERRA is dominated by the summer months, with the largest amount of 2.8 cm $month^{-1}$ occurring in July and more consistent amounts of 1.1–1.5 cm $month^{-1}$ over the winter period, from November to May. For the north polar cap, the precipitable water tendency term is significant in the seasonal cycle and results in a 1-month delay between the maxima in convergence (July) and net precipitation (August). Also shown in Fig. 3a are the separate MERRA precipitation and evaporation curves from physics output. Evaporation is plotted as the negative to show the summation resulting in $P - E$. Evaporation reaches a maximum of 1.9 cm $month^{-1}$ in May, which is concurrent with the high-latitude melt season, and again becomes as large as 1.6 cm $month^{-1}$ in October with the reintroduction of winter conditions over a large open water fraction persisting from summer. While the overall

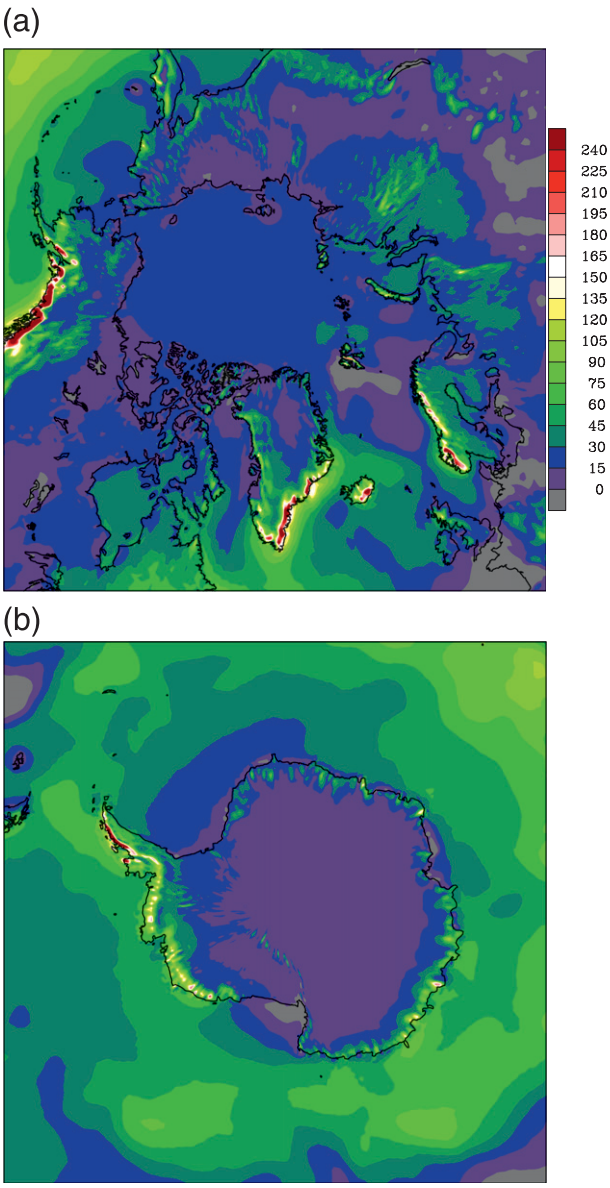

FIG. 2. Contours of 1979–2005 MERRA atmospheric moisture convergence for high latitudes for (a) the Northern Hemisphere and (b) the Southern Hemisphere. Contour interval is 15 cm yr^{-1}.

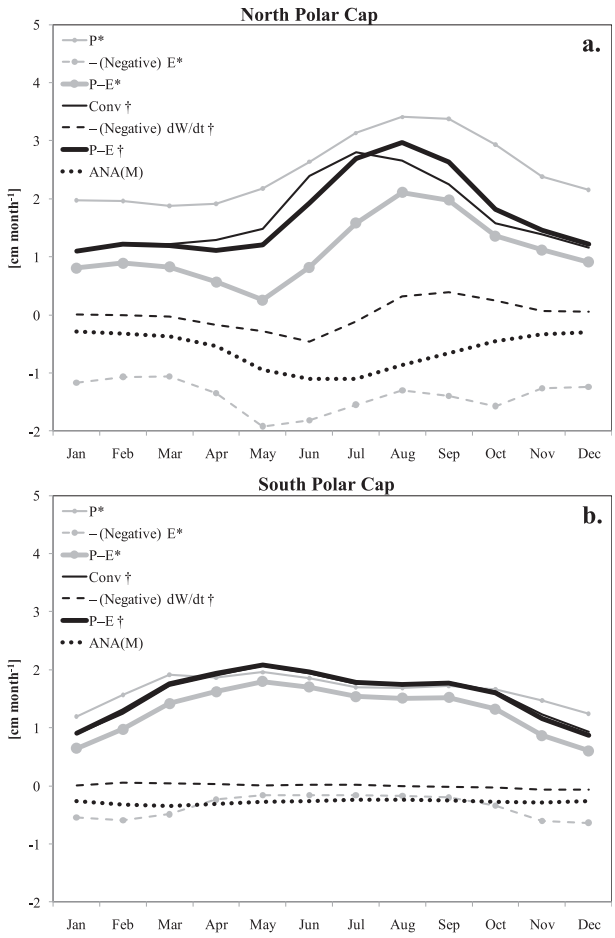

FIG. 3. Average annual time series for MERRA surface moisture flux components (cm month^{-1}) for (a) the north polar cap and (b) the south polar cap. Values using aerological analysis fields are denoted by a dagger, and physics output fields are denoted by asterisks.

shape of the physics output $P - E$ time series curve (denoted by thick gray) is generally reflective of precipitation, it is also strongly influenced by the maximum in evaporation in May.

The difference between the aerological and physics output net precipitation curves corresponds to the analysis increment quantity $\mathrm{ANA}_{(M)}$. The negative value for $\mathrm{ANA}_{(M)}$ indicates the aerological $P - E$ is greater than the physics output value. Compared to the mean moisture convergence field shown in Fig. 2a, MERRA physics output $P - E$ values are less than 15 cm yr^{-1} over most of the central Arctic Ocean, Siberia, and central Canada, with spurious negative values over the Mackenzie River basin and small areas of Siberia and Alaska. Both estimates of net precipitation are produced by the GEOS data assimilation system that has been incrementally adjusted to a 6-hourly observation-based field. However, surface fluxes, such as precipitation and evaporation, are more heavily dependent on the physical parameterizations of the model than the aerological field. For the north polar cap, $\mathrm{ANA}_{(M)}$ is significant in MERRA and ranges from −0.3 cm month^{-1} in January to −1.1 cm month^{-1} in June. The 1979–2005 average for the analysis increments $\mathrm{ANA}_{(M)}$ is −7.3 cm yr^{-1} (1.6 cm yr^{-1} standard deviation from annual values). The agreement between the two time series of $P - E$ in Fig. 3a are comparable to NCEP–National Center for Atmospheric Research (NCAR; Kalnay et al. 1996) and the 15-yr ECMWF Re-Analysis (ERA-15; Gibson et al. 1997) aerological and prognostic curves shown in Bromwich et al. (2000).

TABLE 1. MERRA average surface moisture flux components (cm yr^{-1}) for Northern Hemisphere polar regions in comparison with previous results. The standard deviation of annual values is shown in parentheses.

	Source	Period	P	E	$P - E$*	$P - E$**
70°–90°N	MERRA	1979–2005	29.9 (1.6)	16.7 (0.7)	13.2 (1.6)	20.5 (1.5)
(North polar cap)	MERRA	1979–97	29.5 (1.3)	16.8 (0.8)	12.8 (1.3)	20.9 (1.5)
	MERRA	1999–2005	31.5 (1.1)	16.6 (0.4)	14.8 (1.0)	19.8 (1.1)
	CFSR	1979–2005	42.3 (1.9)	18.6 (0.8)	23.7 (1.6)	
	ERA-I	1989–2005	31.9 (1.4)	14.0 (1.0)	17.9 (1.5)	
	Bromwich et al. (2000)	1979–93				18.9 (2.3)
	Jakobson and Vihma (2010)	1979–2001	32.3 (2.3)	14.4 (0.9)	17.9 (2.0)	19.2 (1.6)
	Groves and Francis (2002)	1979–98				15.1
	Serreze et al. 1995	1974–91				16.3
Arctic Ocean	MERRA	1979–2005	28.5 (1.7)	15.0 (0.8)	13.5 (1.7)	21.3 (1.7)
	MERRA	1979–97	28.3 (1.5)	15.1 (0.8)	13.1 (1.5)	21.8 (1.6)
	MERRA	1999–2005	29.7 (1.5)	14.8 (0.6)	14.9 (1.2)	20.2 (1.5)
	CFSR	1979–2005	41.3 (2.3)	17.1 (1.0)	24.2 (2.1)	
	ERA-I	1989–2005	30.3 (1.9)	12.5 (1.1)	17.8 (1.8)	
	Serreze et al. (2006)	1979–2001	31.0	13.0	19.0	21.0 (2.1)
Greenland Ice Sheet	MERRA	1979–2005	43.4 (4.6)	0.9 (0.2)	42.4 (4.7)	45.9 (4.4)
	MERRA	1979–97	41.9 (4.5)	1.0 (0.1)	41.0 (4.5)	44.8 (4.4)
	MERRA	1999–2005	47.4 (2.2)	0.6 (0.1)	46.8 (2.2)	49.6 (1.8)
	CFSR	1979–2005	49.3 (4.2)	7.8 (0.6)	41.5 (4.0)	
	ERA-I	1989–2005	42.2 (3.4)	2.5 (0.2)	39.8 (3.5)	
	Burgess et al. (2010)	1979–2005			34.4 (2.3)	
	Ettema et al. (2009)	1958–2007	43.4 (2.3)	1.5	41.9	

* Computed using physics output fields.
** Computed using aerological method.

For the Southern Hemisphere polar region, the mean surface moisture flux is strongly influenced by the topographic barrier of the Antarctic Ice Sheet. As shown in Fig. 2b, this results in a strong gradient in the averaged moisture convergence along the East Antarctic coastal escarpment, with large values found in coastal Wilkes Land of greater than 90 cm yr^{-1}. Amounts of greater than 100 cm yr^{-1} are seen in coastal regions of the West Antarctic Ice Sheet, and the largest mean values of up to 162 cm yr^{-1} are found along the western coast of the Antarctic Peninsula. Negative contours are confined to the southwestern Ross Sea and offshore of Mac Robertson Land near Mawson Station (68°S, 63°E). The polar desert of the East Antarctic Plateau is indicated by the vast area of the interior ice sheet receiving less than 15 cm yr^{-1}. Qualitatively, this region extends farther north than is found in other studies, but the plateau is devoid of spurious negative values in the long-term average that are found to afflict other datasets (see, e.g., Tietäväinen and Vihma 2008). Over the adjacent Southern Ocean, values of up to 82 cm yr^{-1} are located equatorward of Victoria Land, while smaller quantities are found in the eastern Pacific sector; amounts of less than 30 cm yr^{-1} are found in the southern Weddell Sea. The general features of Fig. 2b are plausible for the Southern Hemisphere. For example, ERA-40 moisture convergence for the period 1979–2001 similarly indicates large amounts in the Southern Ocean north of Victoria Land and smaller values over the ocean in the South Pacific sector adjacent to West Antarctica (Tietäväinen and Vihma 2008). For the averaged annual time series, the largest surface moisture flux values over the south polar cap in MERRA occur in winter (Fig. 3b), with a maximum in May of 2.1 cm $month^{-1}$ and a minimum of 0.9 cm $month^{-1}$ in December. Figure 3b indicates a suggestion of the semiannual oscillation in the aerological $P - E$ with a second maximum of 1.8 cm $month^{-1}$ in September. In contrast to the north polar cap, the precipitable water tendency or storage term on monthly time scales is essentially zero. Evaporation from MERRA physics output is less than 0.2 cm $month^{-1}$ during winter months April–September, but it reaches 0.6 cm $month^{-1}$ during summer months, which is half of the precipitation value in December and January.

The area-averaged components of the surface moisture flux for the north polar cap and other regions from MERRA are presented in Table 1 for the period 1979–2005. As noted previously, the difference for the 70°–90°N domain of 7.3 cm yr^{-1} between MERRA aerological and physics output estimates is large but comparable to that found by Bromwich et al. (2000) for ERA-15 and NCEP–NCAR reanalyses over the period 1979–1993. Serreze et al. (2006) and Jakobson and Vihma (2010) noted a substantially smaller imbalance in

ERA-40 between aerological and prognostic estimates of 1.4 cm yr^{-1} for the period 1979–2001. For the north polar cap, the MERRA aerological $P - E$ (denoted by ** in Table 1) is larger than most of the recent estimates tabulated by Bromwich et al. (2000); however, is within the standard deviation. Of particular note is Serreze et al. (1995), who did not use reanalyses but rather employed the aerological method using the untreated observations of the rawinsonde network and obtained a value of 16.3 cm yr^{-1}. More recently, Groves and Francis (2002) produced a north polar cap estimate using satellite-retrieved moisture profiles and NCEP–NCAR reanalysis winds of 15.1 cm yr^{-1} for the period 1979–1998, while Jakobson and Vihma (2010) computed 19.2 cm yr^{-1} using ERA-40 aerological values for the period 1979–2001. Given the interannual variability, MERRA compares reasonably well to these previous estimates.

Also shown in Table 1 are corresponding model output values for the ERA-I and for CFSR for the north polar cap over available overlapping years. MERRA net precipitation from physics output is less than the other two reanalyses. Notably, the CFSR prognostic $P - E$ exceeds the MERRA physics output value by about 80% and the MERRA aerological value by 16%. Most of this difference is associated with CFSR precipitation, which is larger than MERRA and ERA-I for all months of the year. For February, MERRA and ERA-I precipitation both average 2.0 cm $month^{-1}$ over concurrent years 1989–2005, while CFSR averages 2.7 cm $month^{-1}$. For August, the CFSR averages 5.1 cm $month^{-1}$, which compares to 3.9 cm $month^{-1}$ for ERA-I and 3.5 cm $month^{-1}$ for MERRA. Differences between MERRA and ERA-I are associated with evaporation. All three products have a semiannual cycle in evaporation similar to that shown in Fig. 3a for MERRA; however, the phase and amplitude differ among the reanalyses for concurrent years. In particular, CFSR and MERRA place the springtime maximum in May, while the ERA-I is consistently one month later, and the CFSR indicate much larger evaporation in October than the other two reanalyses. Average evaporation values for October are 2.3 cm $month^{-1}$ for the CFSR, 1.5 cm $month^{-1}$ for the ERA-I, and 1.6 cm $month^{-1}$ for MERRA.

For the Arctic Ocean domain, Serreze et al. (2006) determined ERA-40 values for the period 1979–2001 of 31.0 cm yr^{-1} for model forecast precipitation and 13.0 cm yr^{-1} for prognostic evaporation, yielding a net precipitation value of 19.0 cm yr^{-1}. These values compare with MERRA estimates of 28.5 cm yr^{-1} for physics output precipitation and 15.0 cm yr^{-1} for physics output evaporation, yielding 13.5 cm yr^{-1} net precipitation for the comparable Arctic Ocean domain shown in Fig. 1. Thus, MERRA precipitation and evaporation estimates from this study and ERA-40 values from Serreze et al. (2006) differ significantly as shown in Table 1. The discrepancy in evaporation is examined further in Cullather and Bosilovich (2011, manuscript submitted to *J. Climate*) in the discussion of MERRA energy fluxes. The use of a prescribed sea ice albedo in MERRA results in large biases in shortwave fluxes in May, which leads to compensation by turbulent energy fluxes. Despite these differences in model-derived values, the aerological estimates of net precipitation are nearly equivalent: 21.0 cm yr^{-1} for ERA-40 versus 21.3 cm yr^{-1} for MERRA. Using satellite-derived moisture estimates, Groves and Francis (2002) determined a net precipitation value over a similar Arctic domain of 14.5 cm yr^{-1} and tabulated $P - E$ estimates from other sources ranging from 10.5 to 19.5 cm yr^{-1}. These estimates are smaller than both ERA-40 and MERRA aerological values.

A useful source of in situ Arctic Ocean precipitation data are the measurements obtained by Russian ice drifting stations (Colony et al. 1998). These gauge-measured daily observations cover the period 1950–1991 and were obtained from manned stations distributed in the central Arctic that were subject to the movement of drifting ice floes. Daily values have been made available by the National Snow and Ice Data Center (NSIDC). The amounts reported have not been bias corrected for wind-induced undercatch and trace reporting (Yang 1999). Comparisons have been made to MERRA with nine stations that were functioning during the period overlapping with MERRA from 1979 to 1991. The nearest MERRA grid point is used for daily comparisons, and MERRA amounts are summed over 24 hourly values. As has been found with previous evaluations with reanalyses, temporal comparisons using daily values are challenging because of the episodic nature of the observations and trace precipitation reporting (Bromwich et al. 2000). Approximately 40% of all ice drifting station reports indicate zero precipitation. In contrast, 56% of corresponding MERRA daily values range between 0.1 and 0.5 mm day^{-1} water equivalent. There is also some ambiguity regarding the time definitions for the station values. Temporal averaging produces some agreement between station observations and MERRA. A representative example is shown in Fig. 4 using a synoptic (7 days) running mean for station NP-30, which was located near the international date line between 74° and 84°N and reported over a period of 1200 days. The correlation of the two time series shown in Fig. 4 is 0.74. Monthly averages are computed for each station for months of more than 20 observing days, resulting in 119 points for comparison. This averaging indicates an annual MERRA bias of 11%. The bias is seasonal and

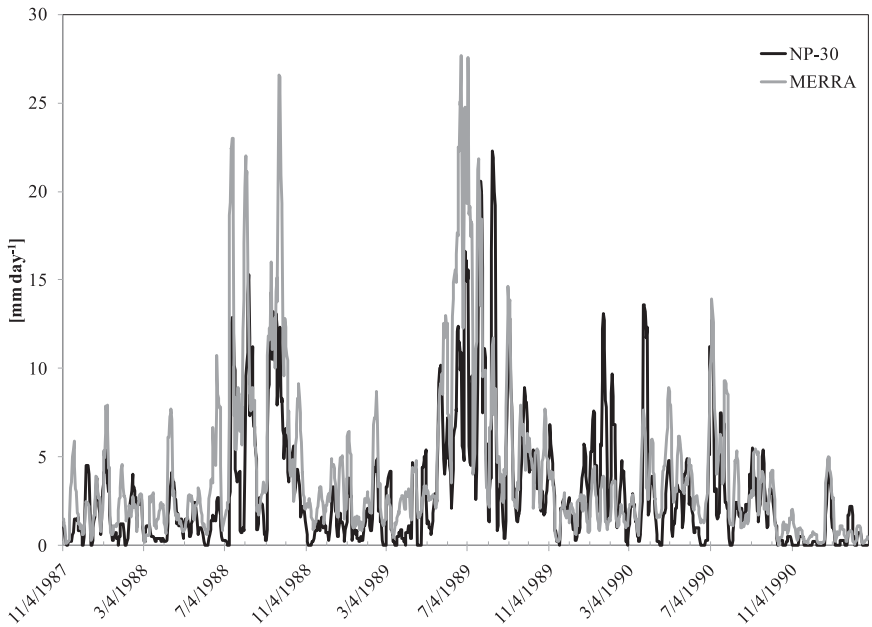

FIG. 4. Comparison of MERRA with NP-30 Arctic drifting station daily gauge precipitation for a 7-day running mean (mm day^{-1}).

produces MERRA overestimates averaging greater than 60% in April–June but less than 2% for other months. Given the gauge biases computed by Yang (1999), the temporal agreement on time scales of greater than a few days is suggested to be reasonable.

Estimates of the surface moisture flux for the south polar cap and Antarctica are given in Table 2. For comparison to the south polar cap $P - E$, Genthon and Krinner (1998) computed values using ERA-15 for the period 1979–93 of 16.2 and 14.5 cm yr^{-1} for aerological and prognostic methods, respectively, while Tietäväinen and Vihma (2008) determined an aerological value from ERA-40 of 17.4 cm yr^{-1} over the period 1979–2001. MERRA values shown in Table 2 are within this broad range of previous estimates. Additional comparisons are made for the conterminous Antarctic grounded ice sheet domain as shown in Fig. 1. Monaghan et al. (2006) tabulated estimates from previous studies for the base period 1985–2001, as well as their results using a polar version of the fifth-generation Pennsylvania State University–NCAR Mesoscale Model (MM5) with ERA-40 and NCEP reanalyses forcing on lateral boundaries. Using ERA-40 forcing, Monaghan et al. determined a $P - E$ value of 18.0 cm yr^{-1} with a standard deviation of 0.8 cm yr^{-1} and presented estimates from other sources ranging from 13.5 to 15.7 cm yr^{-1}. A value of 8.4 cm yr^{-1} is given for the NCEP reanalyses' prognostic output, but this was discounted by Monaghan et al. because of an unrealistically large quantity for E. Corresponding MERRA $P - E$ values for the 1985–2001 period are 16.7 cm yr^{-1} for the aerological method and 15.0 cm yr^{-1} from physics output.

Also shown in Table 2 are corresponding values for the CFSR and ERA-I for the south polar cap. Similar to the north polar cap, the CFSR prognostic P, E, and $P - E$ are much larger than for the other two reanalyses, while MERRA and ERA-I principally differ in E. The CFSR forecast precipitation exceeds MERRA by 41% and ERA-I by 33%. Over the averaged annual cycle, these differences are largest in summer. Average precipitation in January for the concurrent period 1989–2005 is 2.0 cm month^{-1} for the CFSR, 1.4 cm month^{-1} for ERA-I, and 1.2 cm month^{-1} for MERRA. For evaporation, the CFSR is larger than the other two reanalyses throughout the annual cycle, while MERRA evaporation is larger than ERA-I for winter months and less than ERA-I in December and January. As precipitation dominates evaporation over the south polar cap, differences in net precipitation are largely reflective of the differences in P. While the CFSR prognostic net precipitation value is much larger than the corresponding value for MERRA physics output, it agrees with the MERRA aerological estimate of 19.4 cm yr^{-1}.

b. Analysis increments

The spatial distribution of the variable $\mathrm{ANA}_{(M)}$ from MERRA in the Arctic is shown in Fig. 5a. The pattern is complex at lower latitudes, with large positive and negative values in close proximity over western Europe. For the Arctic, there is some correlation between the spatial

TABLE 2. As in Table 1, but for the Southern Hemisphere.

	Source	Period	P	E	$P - E$[a]	$P - E$[b]
70°–90°S	MERRA	1979–2005	19.8 (1.4)	4.3 (0.2)	15.5 (1.3)	18.8 (1.1)
(South polar cap)	MERRA	1979–97	19.2 (0.9)	4.3 (0.1)	14.9 (0.9)	18.7 (1.1)
	MERRA	1999–2005	21.5 (1.2)	4.3 (0.3)	17.1 (1.0)	19.4 (1.1)
	CFSR	1979–2005	28.0 (0.9)	8.6 (0.9)	19.4 (1.2)	
	ERA-I	1989–2005	21.0 (0.9)	4.3 (0.2)	16.7 (0.7)	
	Genthon and Krinner (1998)	1979–93				16.2
Antarctic Ice sheet	MERRA	1979–2005	16.5 (1.0)	1.1 (0.1)	15.4 (1.1)	17.1 (1.1)
	MERRA	1979–97	16.1 (0.8)	1.1 (0.09)	15.0 (0.8)	16.8 (1.0)
	MERRA	1999–2005	17.5 (1.1)	1.1 (0.05)	16.4 (1.1)	17.8 (1.0)
	CFSR	1979–2005	19.7 (0.9)	3.8 (0.2)	15.9 (0.9)	
	ERA-I	1989–2005	16.7 (0.9)	2.2 (0.1)	14.5 (0.9)	
	Monaghan et al. (2006)	1985–2001	20.0		18.0 (0.8)	
	Arthern et al. (2006)	Long term				14.3 (0.4)[c]
	van de Berg et al. (2006)	1980–2004				17.1 (0.3)[c]
Southern Ocean	MERRA	1979–2005	61.8 (5.9)	26.7 (0.6)	35.1 (6.2)	44.9 (1.8)
	MERRA	1979–97	58.7 (1.9)	26.9 (0.5)	31.8 (2.1)	44.7 (1.9)
	MERRA	1999–2005	70.8 (3.5)	26.2 (0.3)	44.6 (3.5)	45.7 (1.7)
	CFSR	1979–2005	89.7 (2.6)	35.5 (2.7)	54.1 (3.3)	
	ERA-I	1989–2005	67.0 (1.7)	24.6 (0.7)	42.4 (1.7)	

[a] Computed using physics output fields.
[b] Computed using aerological method.
[c] Accumulation.

distribution of $ANA_{(M)}$ and the moisture convergence, with larger magnitudes of greater than $(-)12$ cm yr^{-1} over the North Pacific storm track and smaller values from 0 to $(-)8$ cm yr^{-1} in Siberia and central Canada. It may be noted that the location of individual rawinsonde stations may be discerned in Fig. 5a for coastal Greenland by closed contours, where a large-scale negative field from -4 to -8 cm yr^{-1} is embedded with the zero contour line at stations locations.

The annual cycle shown in Fig. 3a and the spatial pattern of the analysis increments in Fig. 5a evolve over the 1979–2005 period. Of particular interest is the introduction of data from the Advanced Microwave Sounding Unit (AMSU) in November 1998, which has a significant global impact on MERRA (Bosilovich et al. 2011). For the north polar cap, the magnitude of $ANA_{(M)}$ becomes notably smaller after the introduction of AMSU. For the years 1979–97, $ANA_{(M)}$ averages -8.1 cm yr^{-1}. This magnitude is reduced to -4.9 cm yr^{-1} for the years 1999–2005. The impact of these abrupt changes may be seen in the MERRA averages given in Table 1 for years before and after the introduction of AMSU data in 1998. The periods prior to and after the introduction of AMSU may comprise changes associated with trends or interannual variability. However, it is seen in Table 1 that the difference between the MERRA aerological and physics output $P - E$ values has changed between these two periods: this is the impact of the change in the observing system. As seen in Table 1, this change is principally redistributed to P in the balance equation, which increases by 2.0 cm yr^{-1}, and to a lesser degree to other components of the moisture budget. Coastal Greenland upper-air stations are not evident in the $ANA_{(M)}$ field after 1998.

For the south polar cap, as shown in Fig. 3b, the analysis increment $ANA_{(M)}$ is seasonally invariant and is less than 0.3 cm month^{-1}, which is approximately 30% of the surface moisture flux in December and January and 11% in winter months. The spatial distribution of $ANA_{(M)}$ for the Southern Hemisphere, shown in Fig. 5b, is roughly correlated with the patterns of the mean moisture convergence field (Fig. 2b). Figure 5 is contoured at the native spatial resolution of MERRA. East Antarctic coastal upper-air stations are readily apparent in the $ANA_{(M)}$ field, with a larger contrast between values at station locations and the neighboring field than is shown for Greenland. For comparison, Tietäväinen and Vihma (2008) determined a budget residual between aerological and prognostic $P - E$ estimates for the Antarctic continent from ERA-40. Tietäväinen and Vihma (2008) indicate a larger residual for ERA-40, including values greater than 20 cm yr^{-1} in coastal areas and the Antarctic Peninsula region, than is shown for $ANA_{(M)}$ in MERRA. As seen in Fig. 5b, the magnitude of the MERRA analysis increments averages less than 8 cm yr^{-1} over most of the Antarctic continent and 12–16 cm yr^{-1} adjacent to the peninsula. Similar to the Northern Hemisphere, there is a marked decrease in the magnitude of $ANA_{(M)}$ after the

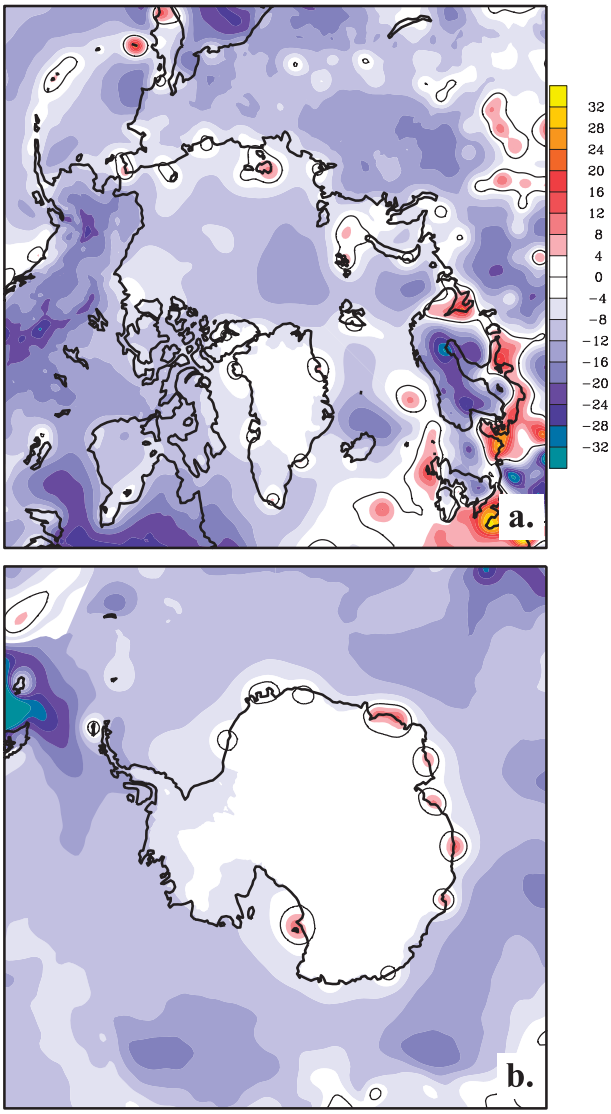

FIG. 5. Contours of 1979–2005 average MERRA analysis increments field for the surface moisture balance for (a) the Northern Hemisphere and (b) the Southern Hemisphere. Contour interval is 4 cm yr^{-1}. Solid black line represents the 0 contour.

introduction of AMSU in November 1998. The analysis increment averages −3.7 cm yr^{-1} for the period 1979–97 but −2.2 cm yr^{-1} for the period 1999–2005. Similar to the north polar cap, this reduction of the analysis increment in the balance equation largely affects P, which increases by 2.2 cm yr^{-1} between the two periods (Table 2). As with Greenland, closed contours associated with coastal stations in the $ANA_{(M)}$ field become less apparent after 1998.

The MERRA analysis increment field denotes differences between analyzed variables and the physical parameterizations of the assimilating GEOS-5 forecast model. These differences are significant in coastal regions of major ice sheets where individual upper-air stations are discernible prior to 1998. This indicates a disagreement in the assimilation of satellite radiances and/or the climate of the assimilating model first-guess field with available rawinsonde data. An area of further interest in this regard is the Southern Ocean region as defined in Fig. 1b. The region lies upstream of Antarctic coastal stations and is essentially devoid of routine in situ observations (Giovinetto et al. 1992). The time series of net precipitation from aerological and physics output methods is shown in Fig. 6a, with the 1979–2005 mean annual cycle from the aerological method subtracted from both curves. The MERRA physics $P - E$ curve indicates a 40% step-function increase in November 1998, from an annual mean of 31.7 to 44.5 cm yr^{-1}, while the aerological value increases only slightly from 44.5 cm yr^{-1} prior to the introduction of AMSU in November 1998 to 45.6 cm yr^{-1} thereafter. The result is a marked decrease in the magnitude of the $ANA_{(M)}$ term for the moisture budget. The difference in the two curves in Fig. 6a is then interpreted as an enhanced sensitivity to the GEOS-5 physical parameterizations as compared to the analysis state and dynamic fields for the Southern Ocean with the introduction of AMSU data. The step change in November 1998 is more substantial at lower latitudes of the Southern Ocean domain and during summer months. As seen in Fig. 6a, the introduction of other sensor data produces less significant changes to the MERRA time series with the exception of the Atmospheric Infrared Sounder (AIRS) in October 2002. The adjustment term changes as follows: from an average of −12.8 cm yr^{-1} prior to the introduction of AMSU to −2.2 cm yr^{-1} from November 1998 to September 2002 to −0.2 cm yr^{-1} from October 2002 through 2005 after the introduction of AIRS. Transitions associated with changes to the observing system are present in other locations (Bosilovich et al. 2011) and MERRA variables, including aerological variables, but not to the extent shown for the Southern Ocean. It is speculated that this is due to the number of in situ observations present in other locations that better constrain the analysis fields. Shown in Figs. 6b and 6c are corresponding time series for the north and south polar caps, respectively, with the 1979–2005 mean annual cycle from the aerological method subtracted from both curves. For the north polar cap, the spring and summer differences between aerological and physics output $P - E$ are apparent as a repeating annual cycle in the physics output anomaly (dark solid curve). After 1998, the magnitude of this difference is reduced over the summer period. The August average of $ANA_{(M)}$ is (−)10.3 cm $month^{-1}$ for the period 1979–97 and (−)3.8 cm $month^{-1}$ for 1999–2005.

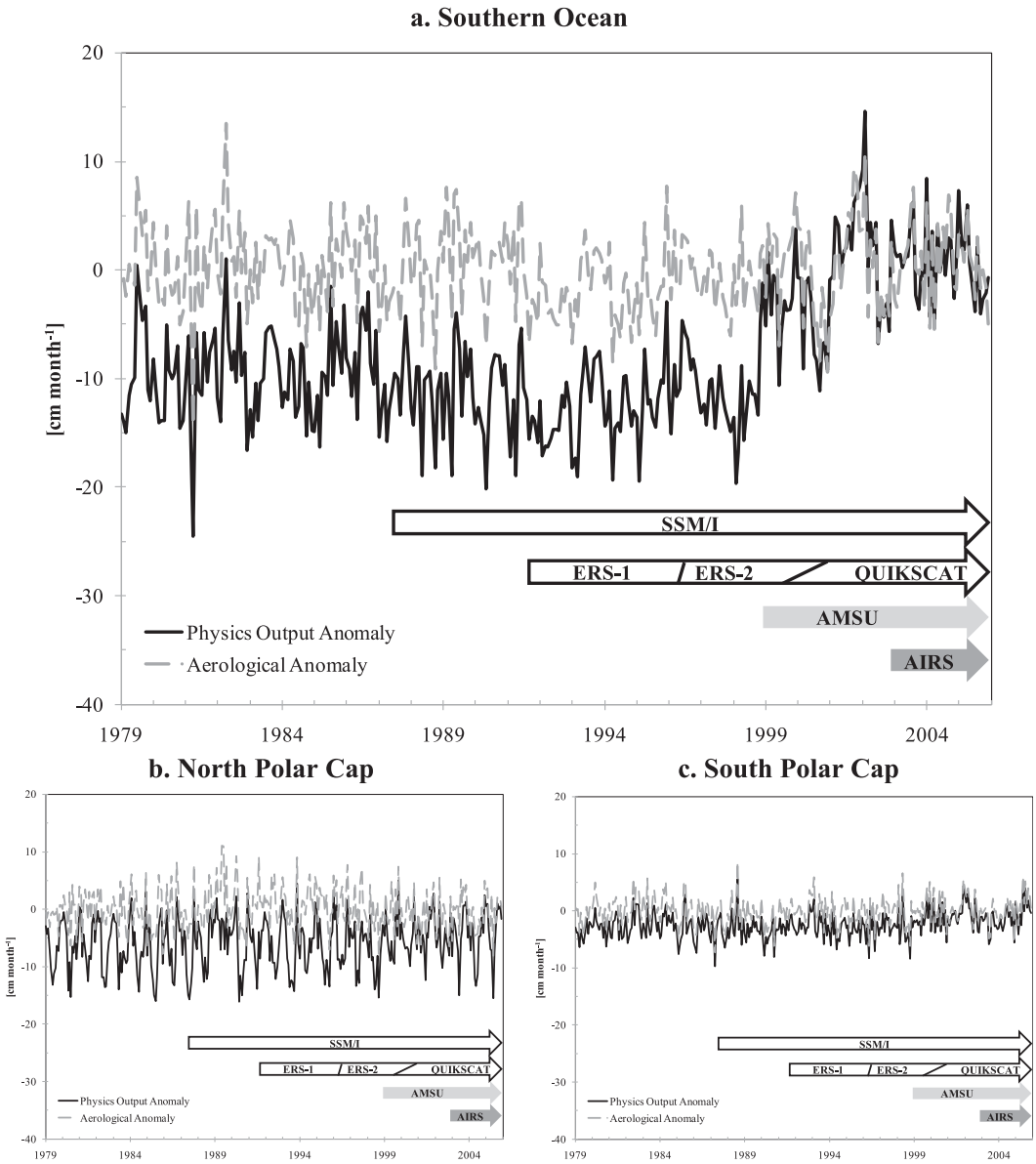

FIG. 6. MERRA net precipitation monthly anomaly (cm month^{-1}) for (a) the Southern Ocean domain, (b) the north polar cap, and (c) the south polar cap based on physics output fields (solid line) and the aerological method (dashed). Anomaly for each curve is referenced to the aerological method for the period 1979–2005. Arrows indicate the timing of input data for select instruments. Times correspond to the introduction of input data to the assimilation system, which may differ from the time of satellite deployment.

For the south polar cap shown in Fig. 6c, it is seen that the two curves more closely overlap after 1998, as suggested by Table 2. It is further speculated that the reduction of $\mathrm{ANA}_{(M)}$ with time for various locations indicates a greater compatibility of the assimilating model with the present-day observing system. This is not surprising in view of the operational requirements of the assimilation system.

It is of interest to understand whether these changes to the observing system affect other reanalyses. Global averages of P and E from the CFSR indicate a substantial step function in 1998 that has been associated with the introduction of AMSU (Saha et al. 2010). Regionally, the impacts are more difficult to discern, particularly given the prominent, global El Niño–Southern Oscillation event in 1998 (Bell et al. 1999). In this initial study, aerological values have not been computed for the CFSR or the ERA-I. For the data-sparse Southern Ocean, it may be noted that CFSR forecast evaporation abruptly decreases after 1998, while ERA-I forecast

P decreases. The average for CFSR E is 37.7 cm yr^{-1} for 1989–97 and 31.6 cm yr^{-1} for 1999–2005, while the ERA-I forecast P is 67.5 cm yr^{-1} for 1989–97 and 66.0 cm yr^{-1} for the later period. Changes in the interannual variability of P, E, and $P - E$ from the three reanalyses over the full time series are qualitatively discernible. However, such changes require additional evaluation.

c. Greenland and Antarctic Ice Sheets

For the Greenland Ice Sheet, Table 1 presents MERRA surface moisture flux values averaged over the gridded area shown in Fig. 1 of 1.4×10^6 km^2. This area is defined by locations of greater than 50% land ice fraction as defined in MERRA using the Global Land Cover Characterization dataset (Loveland et al. 2000). For comparison to MERRA flux components, estimates tabulated by Bromwich et al. (1998) of long-term accumulation synthesized from available observations range from 30.2 to 39.5 cm yr^{-1}, and tabulated studies of precipitation from various sources for the late twentieth century range from 27.6 to 39.1 cm yr^{-1}. Box et al. (2006) used a regional atmospheric model calibrated to glaciological observations to obtain estimates of 39.9 cm yr^{-1} (2.1 cm yr^{-1} std dev) for precipitation and 3.8 cm yr^{-1} (0.3 cm yr^{-1} std dev) for evaporation over the period 1988–2004. More recently, Burgess et al. (2010) determined an average accumulation of 33.7 cm yr^{-1} using a high-resolution regional model for the period 1958–2007 that was calibrated with available core data and coastal meteorological observations to remove complex regional biases. The regional model of Burgess et al. (2010) was forced along lateral boundaries by ERA-40 for the period 1958–2002 and ECMWF operational analyses for the period 2002–2007. Annual fields from the Burgess et al. (2010) study have been obtained and regridded to correspond to MERRA estimates for the years 1979–2005. The corresponding accumulation value for Burgess et al. (2010) is 34.4 cm yr^{-1} and is presented in Table 1. Using these studies, MERRA aerological net precipitation is found to exceed previous Greenland Ice Sheet estimates by a range of 6.4–18.3 cm yr^{-1}, with most studies tending toward the former value. Figure 7 presents the average MERRA atmospheric moisture convergence, the accumulation analysis of Burgess et al. (2010), and the difference. Figure 7 emphasizes the disagreement in the high precipitation zones of coastal southern and southeastern Greenland, with differences locally greater than 280 cm yr^{-1} in the southeast. The average spatial distribution of Greenland accumulation determined by Burgess et al. (2010) consists of amounts of less than 18 cm yr^{-1} over the northern interior of the ice sheet, values of up to 73 cm yr^{-1} in western Greenland, and maximum accumulation amounts greater than 270 cm yr^{-1} on the southeastern coast. Average annual moisture convergence from MERRA exceeds 400 cm yr^{-1} for point locations in southeastern Greenland. The accumulation amounts of Burgess et al. (2010) in southeastern Greenland—though less than MERRA—are characterized in the study as being larger than previous estimates. Differences in the local spatial distribution between Burgess et al. (2010) and MERRA—particularly in western Greenland—are also likely associated with the use of GTOPO30 elevation data in MERRA, which were found to be inaccurate and lower by an average of 180 m over the Greenland Ice Sheet as compared to more reliable elevation data (Box and Rinke 2003). However, the discrepancies in GTOPO30 shown in Box and Rinke (2003) would not necessarily account for the more prominent orographic uplift signal in the MERRA $P - E$ fields for coastal Greenland.

In marked contrast to previous studies, a recent effort using a regional model by Ettema et al. (2009) obtained substantially larger coastal accumulation values. Using the Regional Atmospheric Climate Model version 2 (RACMO2) at high spatial resolution and forced at lateral boundaries by ERA-40 and ECMWF operational analyses, Ettema et al. (2009) found an average for $P - E$ over the Greenland Ice Sheet of 41.9 cm yr^{-1} for the period 1958–2007. This intriguing estimate is comparable to MERRA net precipitation values. Additional in situ measurements in southeastern Greenland would appear essential to resolving differences in these studies.

At Summit in central Greenland (72°N, 38°W), MERRA-averaged moisture convergence is 19.1 cm yr^{-1} with a standard deviation of 3.2 cm yr^{-1}, which compares with an observed accumulation of 22 cm yr^{-1} (Bolzan and Strobel 1994). A time series of annual values of MERRA net precipitation estimates averaged over the Greenland Ice Sheet is shown in Fig. 8 in comparison to estimates using the dataset of Burgess et al. (2010). In comparison to the values derived from Burgess et al. (2010), the correlation is 0.67 for the MERRA aerological time series and 0.57 for the MERRA physics values. It may be seen that the difference between the two MERRA time series and the values of Burgess et al. remain stable over the period 1984–97 and increase after 1997. This change in the bias corresponds with the introduction of AMSU and AIRS satellite data streams, although a transition from ERA-40 to ECMWF operational analyses forcing the Burgess et al. regional model may also be important. Averages over a substantial portion of a limited-area model domain are likely to be more representative of the boundary conditions. As compared to the Southern Ocean domain, the MERRA analysis

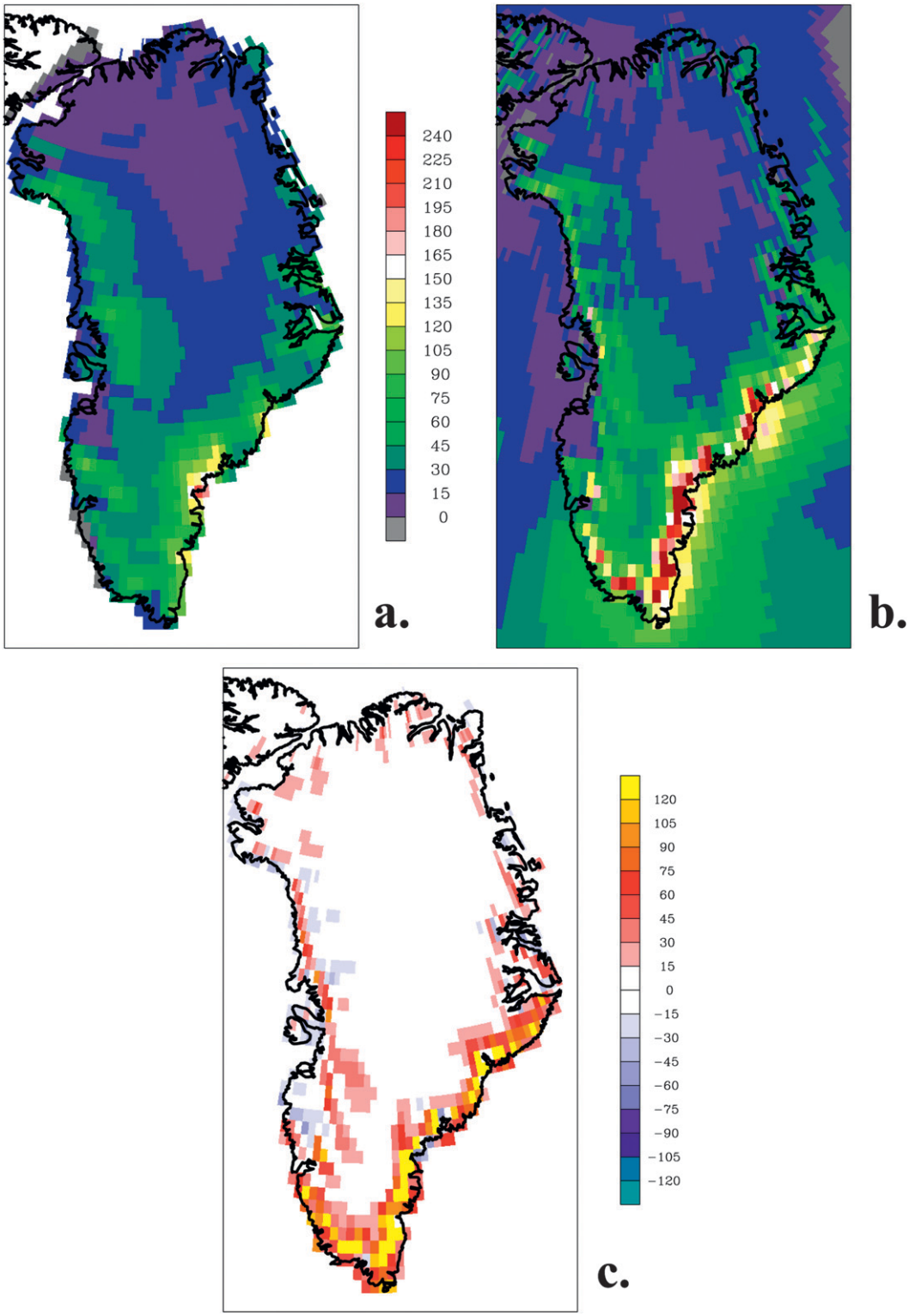

FIG. 7. Gridcell shading of (a) Greenland mesoscale model analysis from Burgess et al. (2010) interpolated to the MERRA grid, (b) MERRA atmospheric moisture convergence, and (c) MERRA moisture convergence–Burgess et al. analysis. Shading interval is every 15 cm yr^{-1}.

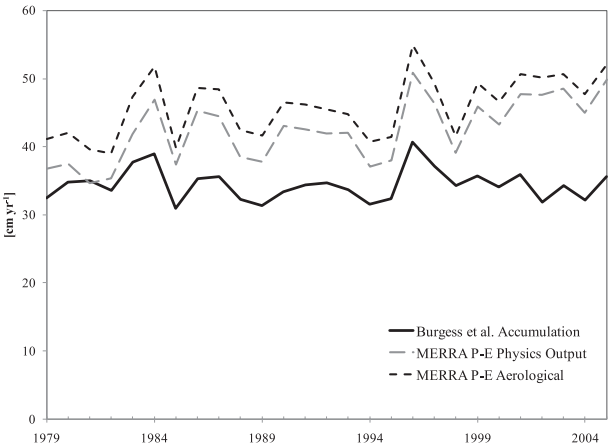

FIG. 8. Comparison of MERRA with Greenland annual accumulation (cm yr^{-1}) synthesis derived from data of Burgess et al. (2010).

increments over Greenland do not change abruptly with the introduction of the satellite data streams, but rather decrease more linearly from 4.5 to 2.5 cm yr^{-1}. As shown in Table 1, both MERRA aerological and physics output values increase over the period prior to and after 1998.

Also shown in Table 1 are corresponding values for CFSR and ERA-I reanalyses. At the available 0.7° × 0.7° resolution, ERA-I prognostic $P - E$ values in southeastern Greenland are greater than those shown for Burgess et al. (2010) but less than corresponding values in Ettema et al. (2009) and MERRA. Amounts of up to 180 cm yr^{-1} are found in the ERA-I $P - E$ averaged for 1989–2005. The annual-averaged CFSR net precipitation field contains values greater than 210 cm yr^{-1} along the southeastern Greenland coast, and the area-averaged net precipitation for the CFSR is comparable to the Ettema et al. (2009) value.

As Monaghan et al. (2006) note, many efforts have been made to produce a long-term validating estimate of Antarctic accumulation but suffer from a sparse surface observational network, remote sensing difficulties, and—where atmospheric models are concerned—incomplete cloud and precipitation microphysics. Recently, Arthern et al. (2006) produced a gridded compilation using available surface observations and satellite data, which is shown in Fig. 9a. The field is interpolated to the MERRA grid from an initial resolution of 100 km × 100 km. This compilation differs from prior efforts in using AMSR-E microwave radiance as a background field for interpolation. Differences with prior methods by Vaughan et al. (1999) and Giovinetto and Zwally (2000) emphasize larger coastal values, particularly along the East Antarctic coastal escarpment and along the Bellingshausen Sea coast in West Antarctica. For comparison, Figs. 9c and 9d show the MERRA aerological and physics output $P - E$. While the large-scale features are similar, the figures illustrate the higher concentration of large amounts in coastal regions in MERRA as compared to the glaciological estimate. In MERRA, the central Antarctic plateau conveyed by the 5 cm yr^{-1} contour is similar to Arthern et al. (2006) but extends farther northward, as noted previously. Not shown, a difference map indicates MERRA aerological $P - E$ is larger than Arthern et al. (2006) accumulation by at least 15 cm yr^{-1} for most coastal areas and is less than the glaciological synthesis by up to 8 cm yr^{-1} in the regions of central Victoria Land to the west of the Transantarctic Mountains, and for locations at higher elevations in West Antarctica. Locally, MERRA is also less than Arthern et al. by more than 15 cm yr^{-1} along the western side of the Lambert Glacier in East Antarctica, the Ellsworth Mountains, and near the highest elevations of the Antarctic Peninsula. These differences correspond to a general view of too much net precipitation along the coast and too little in the interior of the continent in MERRA. These regional differences roughly balance for the continental average, as seen in Table 2. Given that accumulation is a long-term average that also includes other losses, such as wind-blown snow, the differences with MERRA for the conterminous ice sheet average are likely small.

Recently, van de Berg et al. (2006) used the output of RACMO2 calibrated to glaciological observations to determine larger estimates along the Antarctic coast than had been reported previously. As seen in Fig. 9b, the spatial pattern of van de Berg et al. (2006) compares more closely with MERRA aerological $P - E$ than Arthern et al. (2006). The result is entirely analogous to the application to Greenland accumulation by Ettema et al. (2009). Additional measurements and analysis of in situ accumulation estimates for the major ice sheets in coastal and low-elevation regions would seem to be necessary to resolve discrepancies between Arthern et al. (2006) and van de Berg et al. (2006).

4. Summary and discussion

One of the objectives of MERRA is to improve the representation of the water cycle in reanalyses. In general, MERRA provides higher spatial and temporal resolution than earlier reanalyses and provides more temporal continuity (Bosilovich et al. 2011). Among contemporary high-resolution reanalyses, MERRA alone readily provides all of the individual components of the atmospheric moisture budget, including vertical integrals. This represents a significant achievement in assessing the atmospheric hydrologic cycle. MERRA also provides analysis increments for determining local

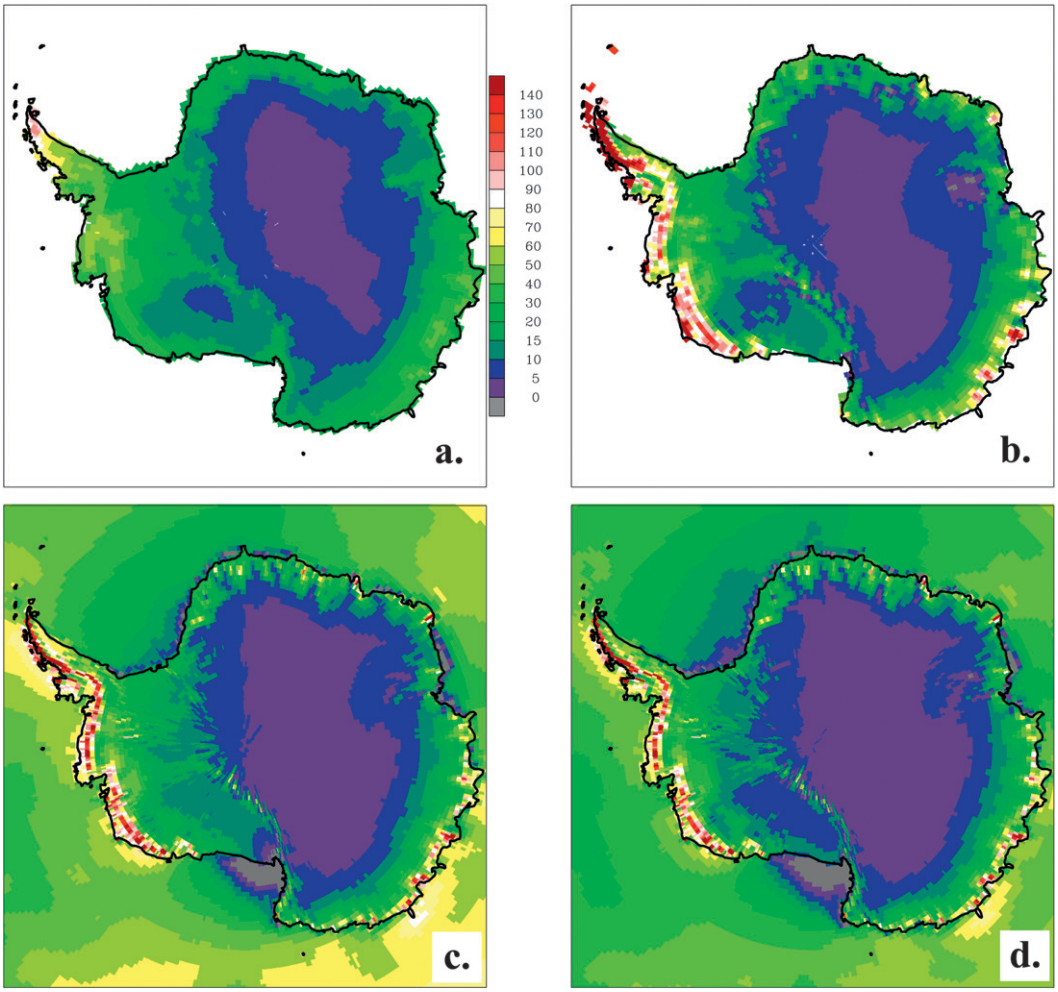

FIG. 9. Gridcell shading of accumulation syntheses from (a) Arthern et al. (2006) and (b) van de Berg et al. (2006), (c) MERRA 1979–2005 atmospheric moisture convergence, and (d) MERRA 1979–2005 physics output $P - E$. All fields are shown at the native resolution of MERRA. The shading interval is every 5 cm yr^{-1} water equivalent over the range 0–20 cm yr^{-1} and every 10 cm yr^{-1} thereafter.

differences between observations and the assimilation model. As noted earlier, reanalyses are restricted by a number of factors, including limitations in the observing system and an incomplete knowledge of the physical processes represented in the background weather forecast model. Examples of these limitations are found in the results presented in this study. However, the available quantification of differences between observations and the assimilating model in MERRA are significant tools for improving our understanding the high-latitude water cycle.

MERRA performs well in representing the high-latitude atmospheric moisture budget in comparison to previous studies and two contemporary reanalyses. As seen in Tables 1 and 2, estimates of the average surface moisture flux ($P - E$) from MERRA aerological output for regional averages are comparable to previous studies. For the Arctic, the analysis increments, or the difference between MERRA aerological and physics output methods, are large but comparable to studies using aerological and prognostic forecast methods with earlier ERA-15 and NCEP–NCAR reanalyses. The difference between MERRA aerological and physics output methods over Antarctica is in contrast relatively small. The spatial patterns of this difference produce signatures of upper-air station locations in coastal regions of major ice sheets, suggesting disagreements between in situ measurements and satellite or background model values. Similar to earlier studies, the aerological estimate in MERRA is persistently larger than corresponding values from physics output in polar regions. This implies that reanalysis model physics are not as

efficient in precipitating atmospheric moisture in high latitudes as would be expected from the atmospheric moisture convergence, or that reanalysis evaporation in polar regions is too large. It is speculated that the latter may be the larger contributor, given difficulties in the Arctic surface energy budget described in Cullather and Bosilovich (2011, manuscript submitted to *J. Climate*). Nevertheless, the modeling of precipitation processes in polar regions remains a significant challenge.

Comparisons with available physics output fields from two contemporary reanalyses and MERRA indicate a large spread of values. Using the average of the physics output entries for MERRA, CFSR, and ERA-I from Tables 1 and 2, the range of values for individual regions is very large. Over Antarctica and the Greenland Ice Sheet, the range is 6% and 14%, respectively. But over the Southern Ocean and Arctic Ocean domains, the range is 43% and 61%, respectively. This range highlights continued problems associated with the representation of cold climate physical processes in global data assimilation models, particularly over high-latitude oceans.

Over the large continental ice sheets of Greenland and Antarctica, the reanalysis surface moisture flux compares well to climatologies to the extent that the validating fields are in agreement. For Greenland, the time series of annual MERRA values for $P - E$ correlates with the limited-area model study of Burgess et al. (2010). This result and others derived from regional climate models (Ettema et al. 2009; van de Berg et al. 2006) should be tempered by the fact that field averages over large regions of a limited-area model domain must necessarily be heavily constrained by the lateral boundary forcing fields, which are numerical analyses. MERRA fields tend to agree more closely with recent studies that place larger moisture flux amounts in close proximity to ice sheet margins and coastlines. Gauge observations over the Arctic Basin taken at submonthly averages are also found to be correlated with the MERRA precipitation time series.

Substantial difficulties with MERRA are apparent. In particular, MERRA is highly sensitive to changes in the satellite-observing system, and this is clearly shown over the data-sparse Southern Ocean, where time series analysis is problematic. The introduction of the AMSU data stream into MERRA in November 1998 produces discontinuities in time series of moisture budget components (Bosilovich et al. 2011). Comparisons indicate that these changes are less significant in the aerological values, as suggested by Fig. 6. This change in the observing system is known to afflict other reanalyses globally (Saha et al. 2010). Discontinuities coinciding with the introduction of AMSU in regional time series for the data-sparse Southern Hemisphere high latitudes are apparent but require further evaluation. The difference between MERRA aerological and physics output methods is also maximum for the spring months in the Arctic, and this is likely related to difficulties associated with the surface energy budget and the sea ice albedo during the melt season. The study highlights the use of the $\mathrm{ANA}_{(M)}$ field for identifying changes to the observing system on both temporal and spatial scales, and for identifying deficiencies in physical parameterizations for the polar regions (Cullather and Bosilovich 2011, manuscript submitted to *J. Climate*).

This study also highlights the need for the reassessment of the surface mass balance of polar ice sheets in coastal margins, as seen by the curious trend of increasing amounts by successive studies. Measurements in these locations are taken in the presence of steep topography and are within close proximity to strong spatial gradients. Difficulties in obtaining accurate in situ accumulation values are detailed in Eisen et al. (2008); however, as they note, more sampling in coastal regions is required for improvement in continental average assessments. Even with reliable point measurements, comparisons to reanalyses are challenging for these areas because of the variable representation of the coastal escarpment in gridded fields. In MERRA, signatures of upper-air stations in the $\mathrm{ANA}_{(M)}$ field in these locations indicate disagreements between in situ measurements and satellite or background model estimates of atmospheric variables. The recent studies cited also suggest higher spatial resolution, such as that afforded by MERRA, is essential for adequately representing the surface moisture flux.

Acknowledgments. The ERA-I data were obtained from the Data Support Section at the National Center for Atmospheric Research. The CFSR data were obtained from the National Operational Model Archive and Distribution System (NOMADS) at the U.S. National Climatic Data Center. Output model fields from Burgess et al. (2010) were obtained from Byrd Polar Research Center, The Ohio State University, Columbus, Ohio. Dataset Arctic Ocean snow and meteorological observations from drifting stations: 1937, 1950–91, version 1.0, was obtained from the National Snow and Data Center (NSIDC), University of Colorado, Boulder. Digitized Antarctic accumulation map of Arthern et al. (2006) was obtained from British Antarctic Survey (BAS), Cambridge, United Kingdom. The Antarctic accumulation map of van de Berg et al. (2006) was obtained from Le Brocq et al. (2010). This study was funded by grants from the NASA Modeling, Analysis, and

Prediction (MAP) Program and the NASA Energy and Water Cycle Study (NEWS) to the second author.

APPENDIX

Representation of the Atmospheric Moisture Budget Using MERRA Variables

The MERRA variables are defined as follows:

DQVDT_DYN	Vertically integrated water vapor tendency for dynamics, kg m^{-2} s^{-1}
DQVDT_PHY	Vertically integrated water vapor tendency for physics, kg m^{-2} s^{-1}
DQVDT_ANA	Vertically integrated water vapor tendency for analysis, kg m^{-2} s^{-1}
DQLDT_DYN	Vertically integrated liquid water tendency for dynamics, kg m^{-2} s^{-1}
DQLDT_PHY	Vertically integrated liquid water tendency for physics, kg m^{-2} s^{-1}
DQLDT_ANA	Vertically integrated liquid water tendency for analysis, kg m^{-2} s^{-1}
DQIDT_DYN	Vertically integrated ice water tendency for dynamics, kg m^{-2} s^{-1}
DQIDT_PHY	Vertically integrated ice water tendency for physics, kg m^{-2} s^{-1}
DQIDT_ANA	Vertically integrated ice water tendency for analysis, kg m^{-2} s^{-1}
EVAP	Surface evaporation, kg m^{-2} s^{-1}
PRECTOT	Total surface precipitation flux, kg m^{-2} s^{-1}
DQVDT_CHM	Vertically integrated water tendency for chemistry, kg m^{-2} s^{-1}
DQVDT_FIL	Artificial filling of water vapor, kg m^{-2} s^{-1}
DQLDT_FIL	Artificial filling of liquid water, kg m^{-2} s^{-1}
DQIDT_FIL	Artificial filling of frozen water, kg m^{-2} s^{-1}

It is noted that a tendency may be expressed as the sum of dynamics, physics, and analysis increment variables denoted by "_DYN," "_PHY," and "_ANA," respectively. For example, the tendency of vertically integrated water vapor (precipitable water) is expressed using MERRA variables as follows:

$$\frac{\partial W_{(v)}}{\partial t} := \mathrm{DQVDT_DYN} + \mathrm{DQVDT_PHY} + \mathrm{DQVDT_ANA}. \tag{A1}$$

For atmospheric moisture, convergence is expressed by the dynamics variables. Equation (1) may then be written using MERRA variables as follows:

$$\begin{aligned}&(\mathrm{DQVDT_DYN} + \mathrm{DQVDT_PHY} + \mathrm{DQVDT_ANA} + \mathrm{DQLDT_DYN} + \mathrm{DQLDT_PHY} + \mathrm{DQLDT_ANA} \\ &\quad + \mathrm{DQIDT_DYN} + \mathrm{DQIDT_PHY} + \mathrm{DQIDT_ANA}) - (\mathrm{DQVDT_DYN} + \mathrm{DQLDT_DYN} + \mathrm{DQIDT_DYN}) \\ &\quad = \mathrm{EVAP} - \mathrm{PRECTOT} + \mathrm{DQVDT_CHM} + (\mathrm{DQVDT_FIL} + \mathrm{DQLDT_FIL} + \mathrm{DQIDT_FIL}) \\ &\quad + (\mathrm{DQVDT_ANA} + \mathrm{DQLDT_ANA} + \mathrm{DQIDT_ANA}).\end{aligned} \tag{A2}$$

REFERENCES

Arthern, R. J., D. P. Winebrenner, and D. G. Vaughan, 2006: Antarctic snow accumulation mapped using polarization of 4.3-cm wavelength microwave emission. *J. Geophys. Res.,* **111,** D06107, doi:10.1029/2004JD005667.

Bell, G. D., M. S. Halpert, V. E. Kousky, M. E. Gelman, C. F. Ropelewski, A. V. Douglas, and R. C. Schnell, 1999: Climate assessment for 1998. *Bull. Amer. Meteor. Soc.,* **80,** S1–S48.

Bintanja, R., 1998: The contribution of snowdrift sublimation to the surface mass balance of Antarctica. *Ann. Glaciol.,* **27,** 251–259.

Bitz, C. M., and Q. Fu, 2008: Arctic warming aloft is data set dependent. *Nature,* **455,** E3–E4.

Bloom, S., L. Takacs, A. DaSilva, and D. Ledvina, 1996: Data assimilation using incremental analysis updates. *Mon. Wea. Rev.,* **124,** 1256–1271.

Bolzan, J. F., and M. Strobel, 1994: Accumulation rate variations around Summit, Greenland. *J. Glaciol.,* **40,** 56–66.

Bosilovich, M. G., F. R. Robertson, and J. Chen, 2011: Global energy and water budgets in MERRA. *J. Climate,* in press.

Box, J. E., and A. Rinke, 2003: Evaluation of Greenland Ice Sheet surface climate in the HIRHAM regional climate model using automatic weather station data. *J. Climate,* **16,** 1302–1319.

——, and Coauthors, 2006: Greenland Ice Sheet surface mass balance variability (1988–2004) from calibrated Polar MM5 output. *J. Climate,* **19,** 2783–2800.

Briegleb, B. P., and D. H. Bromwich, 1998: Polar climate simulations of the NCAR CCM3. *J. Climate,* **11,** 1270–1286.

Bromwich, D. H., R. I. Cullather, Q.-S. Chen, and B. M. Csathó, 1998: Evaluation of recent precipitation studies for Greenland Ice Sheet. *J. Geophys. Res.,* **103,** 26 007–26 024.

——, ——, and M. C. Serreze, 2000: Reanalyses depictions of the Arctic atmospheric moisture budget. *The Freshwater*

Budget of the Arctic Ocean, E. L. Lewis et al., Eds., NATO Science Series 2, Vol. 70, Kluwer Academic Publishers, 163–196.

——, S.-H. Wang, and A. J. Monaghan, 2002: ERA-40 representation of the Arctic atmospheric moisture budget. Workshop on re-analysis, 5-9 November 2001, ERA-40 Project Rep. Series, ECMWF Tech. Rep. 3, 287–298.

Burgess, E. W., R. R. Forster, J. E. Box, E. Mosley-Thompson, D. H. Bromwich, R. C. Bales, and L. C. Smith, 2010: A spatially calibrated model of annual accumulation rate on the Greenland Ice Sheet (1958–2007). *J. Geophys. Res.,* **115,** F02004, doi:10.1029/2009JF001293.

Colony, R., V. Radionov, and F. J. Tanis, 1998: Measurements of precipitation and snow pack at Russian North Pole drifting stations. *Polar Rec.,* **34,** 3–14.

Eisen, O., and Coauthors, 2008: Ground-based measurements of spatial and temporal variability of snow accumulation in East Antarctica. *Rev. Geophys.,* **46,** RG2001, doi:10.1029/2006RG000218.

Ettema, J., M. R. van den Broeke, E. van Meijgaard, W. J. van de Berg, J. L. Bamber, J. E. Box, and R. C. Bales, 2009: Higher surface mass balance of the Greenland Ice Sheet revealed by high-resolution climate modeling. *Geophys. Res. Lett.,* **36,** L12501, doi:10.1029/2009GL38110.

Genthon, C., and G. Krinner, 1998: Convergence and disposal of energy and moisture on the Antarctic polar cap from ECMWF reanalyses and forecasts. *J. Climate,* **11,** 1703–1716.

——, ——, and M. Sacchettini, 2003: Interannual Antarctic tropospheric circulation and precipitation variability. *Climate Dyn.,* **21,** 289–307.

Gesch, D. B., 1994: Topographic data requirements for EOS global change research. U.S. Geological Survey Open-File Rep. 94-626, 60 pp.

Gibson, J. K., P. Kållberg, S. Uppala, A. Hernandez, A. Nomura, and E. Serrano, 1997: ERA description. ERA-15 Project Rep. Series, ECMWF Tech. Rep. 1, 72 pp.

Giovinetto, M. B., and H. J. Zwally, 2000: Spatial distribution of net surface accumulation on the Antarctic Ice Sheet. *Ann. Glaciol.,* **31,** 171–178.

——, D. H. Bromwich, and G. Wendler, 1992: Atmospheric net transport of water vapor and latent heat across 70°S. *J. Geophys. Res.,* **97,** 917–930.

GMAO, 2008: File specification for MERRA products, version 2.1. NASA Tech. Memo., 96 pp. [Available online at http://gmao.gsfc.nasa.gov/products/documents/MERRA_FileSpec.]

Gorshkov, S. G., Ed., 1983: *Arctic Ocean.* Vol. 3, *World Ocean Atlas,* Pergamon, 189 pp.

Grant, A. N., S. Brönnimann, and L. Haimberger, 2008: Recent Arctic warming vertical structure contested. *Nature,* **455,** E2–E3.

Groves, D. G., and J. A. Francis, 2002: Moisture budget of the Arctic atmosphere from TOVS satellite data. *J. Geophys. Res.,* **107,** 4391, doi:10.1029/2001JD001191.

Hines, K. M., D. H. Bromwich, and G. J. Marshall, 2000: Artificial surface pressure trends in the NCEP–NCAR reanalysis over the Southern Ocean and Antarctica. *J. Climate,* **13,** 3940–3952.

Hurrell, J. W., Y. Kushnir, G. Ottersen, and M. Visbeck, 2001: An overview of the North Atlantic Oscillation. *The North Atlantic Oscillation: Climatic Significance and Environmental Impact, Geophys. Monogr.,* Vol. 134, Amer. Geophys. Union, 1–35.

Jakobson, E., and T. Vihma, 2010: Atmospheric moisture budget in the Arctic based on the ERA-40 reanalysis. *Int. J. Climatol.,* **30,** 2175–2194.

Kalnay, E., and Coauthors, 1996: The NCEP/NCAR 40-Year Reanalysis Project. *Bull. Amer. Meteor. Soc.,* **77,** 437–471.

Koster, R. D., M. J. Suárez, A. Ducharne, M. Stieglitz, and P. Kumar, 2000: A catchment-based approach to modeling land surface processes in a general circulation model 1. Model structure. *J. Geophys. Res.,* **105,** 24 809–24 822.

Le Brocq, A. M., A. J. Payne, and A. Vieli, cited 2010: Antarctic dataset in netCDF format. [Available online at http://doi.pangaea.de/10.1594/PANGAEA.734145.]

Loveland, T. R., B. C. Reed, J. F. Brown, D. O. Ohlen, Z. Zhu, L. Yang, and J. W. Merchant, 2000: Development of a global land cover characteristics database and IGBP DISCOVER from 1 km AVHRR data. *Int. J. Remote Sens.,* **21,** 1303–1330.

Monaghan, A. J., and D. H. Bromwich, 2008: Advances in describing recent Antarctic climate variability. *Bull. Amer. Meteor. Soc.,* **89,** 1295–1306.

——, ——, and S.-H. Wang, 2006: Recent trends in Antarctic snow accumulation from Polar MM5 simulations. *Philos. Trans. Roy. Soc.,* **A364,** 1683–1708.

Moody, E. G., M. D. King, S. Platnick, C. B. Schaaf, and F. Gao, 2005: Spatially complete global spectral surface albedos: Value-added datasets derived from Terra MODIS land products. *IEEE Trans. Geosci. Remote Sens.,* **43,** 144–158.

Ogi, M., and J. M. Wallace, 2007: Summer minimum Arctic sea ice extent and the associated summer atmospheric circulation. *Geophys. Res. Lett.,* **34,** L12705, doi:10.1029/2007GL029897.

Reynolds, R. W., N. A. Rayner, T. M. Smith, D. C. Stokes, and W. Wang, 2002: An improved in situ and satellite SST analysis for climate. *J. Climate,* **15,** 1609–1625.

Rienecker, M. M., and Coauthors, 2008: The GEOS-5 Data Assimilation System—Documentation of versions 5.0.1, 5.1.0, and 5.2.0. NASA GSFC Tech. Rep. Series on Global Modeling and Data Assimilation, NASA/TM-2007-104606, Vol. 27, 95 pp.

——, and Coauthors, 2011: MERRA—NASA's Modern Era Retrospective-Analysis for Research and Applications. *J. Climate,* in press.

Rinke, A., and Coauthors, 2006: Evaluation of an ensemble of Arctic regional climate models. Spatiotemporal fields during the SHEBA year. *Climate Dyn.,* **26,** 459–472.

Saha, S., and Coauthors, 2010: The NCEP Climate Forecast System reanalysis. *Bull. Amer. Meteor. Soc.,* **91,** 1015–1057.

Serreze, M. C., R. G. Barry, and J. E. Walsh, 1995: Atmospheric water vapor characteristics at 70°N. *J. Climate,* **8,** 719–731.

——, and Coauthors, 2006: The large-scale freshwater cycle of the Arctic. *J. Geophys. Res.,* **111,** C11010, doi:10.1029/2005JC003424.

Simmons, A. J., S. Uppala, D. Dee, and S. Kobayashi, 2007: ERA Interim: New ECMWF reanalysis products from 1989 onwards. *ECMWF Newsletter,* No. 110, ECMWF, Reading, United Kingdom, 25–35.

Stieglitz, M., A. Ducharne, R. D. Koster, and M. J. Suarez, 2001: The impact of detailed snow physics on the simulation of snow cover and subsurface thermodynamics at continental scales. *J. Hydrometeor.,* **2,** 228–242.

Thompson, D. W. J., and J. M. Wallace, 1998: The Arctic Oscillation signature in the wintertime geopotential height

and temperature fields. *Geophys. Res. Lett.,* **25,** 1297–1300.

Thorne, P. W., 2008: Arctic tropospheric warming amplification? *Nature,* **455,** E1–E2.

Tietäväinen, H., and T. Vihma, 2008: Atmospheric moisture budget over Antarctica and the Southern Ocean based on the ERA-40 reanalysis. *Int. J. Climatol.,* **28,** 1977–1995.

Trenberth, K. E., T. Koike, and K. Onogi, 2008: Progress and prospects for reanalysis for weather and climate. *Eos, Trans. Amer. Geophys. Union,* **89,** 234–235.

Uppala, S. M., and Coauthors, 2005: The ERA-40 Re-Analysis. *Quart. J. Roy. Meteor. Soc.,* **131,** 2961–3012.

van de Berg, W. J., M. R. van den Broeke, C. H. Reijmer, and E. van Meijgaard, 2006: Reassessment of the Antarctic surface mass balance using calibrated output of a regional atmospheric climate model. *J. Geophys. Res.,* **111,** D11104, doi:10.1029/2005JD006495.

Vaughan, D. G., J. L. Bamber, M. Giovinetto, J. Russell, and A. P. R. Cooper, 1999: Reassessment of net surface mass balance in Antarctica. *J. Climate,* **12,** 933–946.

Walsh, J. E., V. M. Kattsov, W. L. Chapman, V. Govorkova, and T. Pavlova, 2002: Comparison of Arctic climate simulations by uncoupled and coupled global models. *J. Climate,* **15,** 1429–1446.

Yang, D., 1999: An improved precipitation climatology for the Arctic Ocean. *Geophys. Res. Lett.,* **26,** 1625–1628.